Atmospheric neutrinos with three flavor mixing

Mohan Narayan, G. Rajasekaran

Institute of Mathematical Sciences, Madras 600 113, India.

S. Uma Sankar

Department of Physics, I.I.T., Powai, Bombay 400 076, India.

(February 1, 2008)

arXiv:hep-ph/9607279v2 26 Feb 1997

Abstract

We analyze the atmospheric neutrino data in the context of three flavor neutrino oscillations taking account of the matter effects in the earth. With the hierarchy among the vacuum mass eigenvalues $\mu_3^2 \gg \mu_2^2 \geq \mu_1^2$, the solution of the atmospheric neutrino problem depends on $\delta_{31} = \mu_3^2 - \mu_1^2$ and the 13 and 23 mixing angles ϕ and ψ. Whereas the sub-GeV atmospheric neutrino data imposes only a lower limit on $\delta_{31} > 10^{-3}$ eV^2, the zenith angle dependent suppression observed in the multi-GeV data limits δ_{31} from above also. The allowed regions of the parameter space are strongly constrained by the multi-GeV data. Combined with our earlier solution to the solar neutrino problem which depends on $\delta_{21} = \mu_2^2 - \mu_1^2$ and the 12 and 13 mixing angles ω and ϕ, we have obtained the ranges of values of the five neutrino parameters which solve both the solar and the atmospheric neutrino problems simultaneously.

I. INTRODUCTION

In recent years, deep underground detectors have been measuring the flux of neutrinos produced in the atmosphere. (Unless explicitly stated, we call neutrinos and anti-neutrinos collectively as neutrinos). These neutrinos are produced from the decays of $\pi^{\pm}$ and $K^{\pm}$ mesons which, in turn, are produced by cosmic ray interactions with the atmosphere. One expects the number of muon neutrinos to be twice the number of electron neutrinos. The predictions of detailed Monte Carlo calculations confirm that the ratio of the flux of muon neutrinos Φ_{ν_μ} to the flux of electron neutrinos Φ_{ν_e} is about 2 [1,2]. The predicted neutrino fluxes from different calculations differ significantly from each other (by as much as 30%), but the predictions for the ratio of the fluxes $\Phi_{\nu_\mu}/\Phi_{\nu_e}$ are in good agreement with each other. The large water Cerenkov detectors Kamiokande and IMB [3] have measured this ratio and have found it to be about half of what is predicted [4]. The experimental results are presented in the form of a double ratio

$$R = \frac{\left(\frac{N_{\nu_\mu}}{N_{\nu_e}}\right)_{obs}}{\left(\frac{N_{\nu_\mu}}{N_{\nu_e}}\right)_{MC}} = \frac{r_{obs}}{r_{MC}}. \tag{1}$$

Kamiokande collaboration have presented their results for neutrinos with energy less than 1.33 GeV (sub-GeV data) [5] and for neutrinos with energy greater then 1.33 GeV (multi-GeV data) [6]. For the sub-GeV data, $R = 0.60^{+0.07}_{-0.06} \pm 0.05$ and for the multi-GeV data, after averaging over the zenith angle, $R = 0.57^{+0.08}_{-0.07} \pm 0.07$. The value of R has no significant zenith angle dependence for the sub-GeV data. However, for the multi-GeV data, R is smaller for large values of zenith angle (upward going neutrinos) and is larger for small values of zenith angle (downward going neutrinos). Kamiokande have analyzed their data assuming that the smaller observed value of R is caused by neutrino oscillations. They have done two independent analyses, one assuming two flavor oscillations between $\nu_\mu \leftrightarrow \nu_e$ and the other assuming two flavor oscillations between $\nu_\mu \leftrightarrow \nu_\tau$. For both the cases, they obtain a mass-squared difference $\delta m^2 \sim 10^{-2} eV^2$ and a mixing angle nearly 45^0. Since the upward going neutrinos travel large distances inside the earth before entering the detector, matter

effects may be important for these, especially at higher energies [7,8]. Therefore one must take matter effects into consideration while analyzing $\nu_\mu \leftrightarrow \nu_e$ oscillations.

Atmospheric neutrino problem was analyzed in the three flavor neutrino oscillation framework previously. In Ref. [9] the sub-GeV data were analyzed under the assumption that one of the mass differences is much smaller than the other. The matter effects due to the passage of neutrinos through the earth were included and the allowed values of neutrino parameters were obtained. Various other authors have analyzed, in the context of three flavor oscillations, accelerator and reactor data in conjunction with the sub-GeV atmospheric data [10] or the multi-GeV data with zenith angle dependence included [11]. However, in both these cases the earth matter effects were not taken into account.

Several authors have attempted a simultaneous solution of the solar and atmospheric neutrino problems in three flavor oscillation scenarios. The solution in Ref. [12] assumes maximal mixing between all the three flavors and derives the constraints on the mass differences. The solution thus obtained restricts the mass difference to be very small ($\sim 10^{-10} \ eV^2$) and is somewhat fine-tuned. Other solutions have assumed the mass hierarchy that was considered in Ref. [9] and obtained the allowed regions in the neutrino parameter space [13–16]. However, all these analyses were based on the sub-GeV atmospheric neutrino data. The multi-GeV data and its zenith angle dependence were not included. In a recent analysis of the multi-GeV data earth matter effects and the zenith angle dependence were taken into account [17]. However, this analysis considered the atmospheirc neutrino problem only.

In this paper, we analyze the Kamiokande multi-GeV data in the framework of three flavor neutrino oscillations. The solar neutrino data and the sub-GeV data of Kamiokande were analyzed earlier in the same framework [16]. We only assume that, of the two mass differences in the problem, the smaller one is chosen to solve the solar neutrino problem and the larger one will be relevant for the atmospheric neutrino problem. We do not, apriori, make any assumption about the form of the mixing matrix. Our starting point is the same as that in Ref. [9]. We include the matter effects due to the passage of neutrinos through the earth. We take the allowed values of neutrino parameters from our earlier work as inputs.

The zenith angle dependent suppression of multi-GeV data places strong further constraints on the parameter space allowed by the solar neutrino problem and the sub-GeV atmospheric neutrino data. In section II, we define our theoretical framework and derive the oscillation probabilities. In section III, we describe the comparison of the theoretical predictions with the Kamiokande data and determine the allowed regions of the neutrino parameters. In section IV we discuss our results and present our conclusions. A brief discussion of the recent LSND result [18] is also included.

II. THEORY

Here we describe the three flavor neutrino mixing and calculate the probability for a neutrino produced as ν_α to be detected as ν_β, where α and β are flavor indices. The flavor eigenstates are related to the mass eigenstates by

$$
\begin{bmatrix} \nu_e \\ \nu_\mu \\ \nu_\tau \end{bmatrix} = U^v \begin{bmatrix} \nu_1^v \\ \nu_2^v \\ \nu_3^v \end{bmatrix}
\tag{2}
$$

where the superscript 'v' denotes vacuum. The unitary matrix U^v can be parametrized as

$$
U^v = U^{23}(\psi) \times U^{phase} \times U^{13}(\phi) \times U^{12}(\omega),
\tag{3}
$$

where $U^{ij}(\theta_{ij})$ is the two flavor mixing matrix between the ith and jth mass eignestates with the mixing angle θ_{ij}. For simplicity, we neglect the CP violation and set $U^{phase} = I$.

In the mass basis the mass-squared matrix is diagonal and can be taken to be

$$
M_0^2 = \begin{bmatrix} \mu_1^2 & 0 & 0 \\ 0 & \mu_2^2 & 0 \\ 0 & 0 & \mu_3^2 \end{bmatrix} = \mu_1^2 I + \begin{bmatrix} 0 & 0 & 0 \\ 0 & \delta_{21} & 0 \\ 0 & 0 & \delta_{31} \end{bmatrix},
\tag{4}
$$

where $\delta_{21} = \mu_2^2 - \mu_1^2$ and $\delta_{31} = \mu_3^2 - \mu_1^2$. Without loss of generality we can take $\mu_3 > \mu_2 > \mu_1$ so that both δ_{21} and δ_{31} are positive. For extreme relativistic neutrinos, the oscillation probability depends only on the mass-squared differences so we ignore the first term $\mu_1^2 I$.

In the flavor basis, the mass-squared matrix is non-diagonal and is given by

$$M_v^2 = U^v M_0^2 \left(U^v\right)^\dagger .$$
(5)

For the propagation of neutrinos through the earth, we need to take the matter effects into account. The charged current scattering between electrons and ν_e induces an effective mass-squared term for ν_e which is of the form $A = 2\sqrt{2} G_F N_e E$, where N_e is the number density of electrons and E is the neutrino energy [19]. This term is present only for the $e - e$ element in the flavor basis so the mass-squared matrix including the matter effects is

$$M_m^2 = M_v^2 + \begin{bmatrix} A & 0 & 0 \\ 0 & 0 & 0 \\ 0 & 0 & 0 \end{bmatrix}.$$
(6)

M_m^2 is a hermitian matirx and can be diagonalized by unitary matrix U^m, which relates the flavor eigenstates to matter dependent mass eigenstates

$$\begin{bmatrix} \nu_e \\ \nu_\mu \\ \nu_\tau \end{bmatrix} = U^m \begin{bmatrix} \nu_1^m \\ \nu_2^m \\ \nu_3^m \end{bmatrix}$$
(7)

where the superscript 'm' stands for matter. We denote the matter dependent mass eigenvalues as m_1, m_2 and m_3. The matter dependent mixing matrix U^m can be parametrized in terms of three mixing angles in a manner similar to that of U^v as given in eq.(3). The matter dependent mass eigenvalues and mixing angles can be obtained, in terms of the vacuum parameters and A, by solving the eigenvalue problem of M_m^2 in eq.(6)

The distance scales and the energy scales in the solar neutrino problem and the atmospheric neutrino problem are very different. Therefore, one needs two distinct mass scales to solve the solar and the atmospheric neutrino problems simultaneously. To satisfy the constraints from all the three solar neutrino experiments, one must choose $\delta_{21} \sim 10^{-5} \ eV^2$, which is roughly the matter term A for the solar neutrinos due to their passage through the sun. As we will shortly see, the sub-GeV atmospheric neutrino data impose a constraint

5

$\delta_{31} \geq 10^{-3}~eV^2$. Hence $\delta_{31} \gg \delta_{21}$. If $\delta_{21} \sim 10^{-5}~eV^2$, the oscillation length corresponding to it, even for the minimum of the atmospheric neutrino energies, is of the order of the diameter of the earth. In the expression for the oscillation probability, δ_{21} can be set to zero. Therefore the oscillations are dependent on only one mass difference δ_{31} in the atmospheric neutrino problem.

In the approximation of neglecting δ_{21}, it is straightforward to show that the oscillation probability is independent of the mixing angle ω. Including matter effects does not alter this conclusion. Note, however, that neglecting δ_{21} does not reduce the problem to an effective two flavor mixing. The three flavor nature of the problem is reflected by the fact that the oscillation probability is a function of the mass difference δ_{31} and *two* mixing angles ϕ and ψ. In the case of an effective two flavor mixing, the oscillation probability is dependent on one mixing angle only. When the matter effects are included the mixing angle ψ remains unaffected but the angle ϕ becomes matter dependent [9],

$$\tan 2\phi_m = \frac{\delta_{31} \sin 2\phi}{\delta_{31} \cos 2\phi - A}. \tag{8}$$

The mass eigenvalue of ν_1^m remains 0 (actually it is of the order of δ_{21} which we are neglecting here). The other two matter dependent mass eigenvalues are given by

$$m_2^2 = \frac{1}{2}\left[(\delta_{31} + A) - \sqrt{(\delta_{31}\cos 2\phi - A)^2 + (\delta_{31}\sin 2\phi)^2}\right] \tag{9}$$

$$m_3^2 = \frac{1}{2}\left[(\delta_{31} + A) + \sqrt{(\delta_{31}\cos 2\phi - A)^2 + (\delta_{31}\sin 2\phi)^2}\right] \tag{10}$$

Equations (8), (9) and (10) are valid for neutrinos. For anti-neutrinos, we get a similar set of formulae with A replaced by $-A$.

The neutrinos produced in the atmosphere enter the earth after travelling through the atmosphere for about 20 Km and finally reach the detector after travelling through the earth. The distance travelled through the earth is a function of the zenith angle. For the five bins considered by Kamiokande [6], the average values of the cosine of the zenith angle are -0.8, -0.4, 0.0, 0.4, 0.8 and the average distances travelled through the earth are 10210, 5137, 832, 34, 6 Km respectively [12].

A neutrino of flavor α, produced in the atmosphere at time $t = 0$, propagates through the atmosphere as a linear combination of the vacuum mass eigenstates. If the neutrino enters earth at time $t = t_1$, its state vector at that time can be written as

$$|\Psi_\alpha(t_1)\rangle = \sum_i U^v_{\alpha i} exp\left(-i\frac{\mu_i^2 t_1}{2E}\right)|\nu_i^v\rangle. \tag{11}$$

Reexpressing the vacuum mass eigenstates in terms of flavor states, we have

$$|\Psi_\alpha(t_1)\rangle = \sum_i U^v_{\alpha i} exp\left(-i\frac{\mu_i^2 t_1}{2E}\right)\sum_\lambda U^{v*}_{\lambda i}|\nu_\lambda\rangle. \tag{12}$$

After entering the earth, the neutrino propagates as a linear combination of the matter dependent mass eigenstates. We take the earth to be a slab of constant density. At the time of detection $t = t_d$, the state vector takes the form

$$|\Psi_\alpha(t_d)\rangle = \sum_i U^v_{\alpha i} exp\left(-i\frac{\mu_i^2 t_1}{2E}\right)\sum_\lambda U^{v*}_{\lambda i}\sum_j U^m_{\lambda j} exp\left(-i\frac{m_j^2(t_d - t_1)}{2E}\right)|\nu_j^m\rangle. \tag{13}$$

Hence the amplitude for the neutrino produced as flavor α at t $= 0$ to be detected as a neutrino of flavor β at time t_d is given by

$$\langle\nu_\beta|\Psi_\alpha(t_d)\rangle = \sum_i \sum_\lambda \sum_j U^v_{\alpha i} U^{v*}_{\lambda i} U^m_{\lambda j} U^{m*}_{\beta j} exp\left(-i\frac{\mu_i^2 t_1}{2E}\right) exp\left(-i\frac{m_j^2(t_d - t_1)}{2E}\right). \tag{14}$$

The probability of oscillation $P_{\alpha\beta}$ is given by the modulus square of the above amplitude. If $t_d - t_1$ is set equal to zero (that is if the total time of travel is equal to the time of travel through the atmosphere) then the expression in eq.(14) reduces to the simple vacuum oscillation amplitude. The same is true if the matter effects are ignored; i.e. if $U^m = U^v$ and $m_i = \mu_i$.

For bins $1, 2$ and 3, the distance travelled in earth is much larger than the distance travelled in the atmosphere. Therefore t_1 is much smaller than t_d for these bins and can be neglected. Neglecting t_1, simplifies the expressions for oscillation probability and we obtain the expressions derived earlier in Ref. [9]. However, for bins 4 and 5, the distance of travel in atmosphere is comparable to that in earth. Therefore t_1 is of the same of order of magnitude as t_d and can not be neglected. Keeping $t_1 \neq 0$ in eq.(14) properly takes into account the non-adiabaticity in the abrupt change in density when the neutrino enters earth.

III. CALCULATION AND RESULTS

A. Sub-GeV Data

First we briefly describe our analysis of the sub-GeV data and highlight the contrast between it and the analysis of the multi-GeV data. Matter effects are unimportant for the sub-GeV data. If the earth is taken to be a slab of density 5.5 gm/cm^3, the matter term A for the sub-GeV neutrinos is less than 3.8×10^{-4} eV^2. As we will shortly see, the sub-GeV data sets a lower limit on $\delta_{31} > 10^{-3}$ eV^2. Hence the matter effects can be neglected and the expressions for $P_{\alpha\beta}$ in the sub-GeV analysis are simply the vacuum oscillation probabilities

$$P^0_{\alpha\beta} = \left(U^v_{\alpha 1}U^v_{\beta 1}\right)^2 + \left(U^v_{\alpha 2}U^v_{\beta 2}\right)^2 + \left(U^v_{\alpha 3}U^v_{\beta 3}\right)^2 + 2\,U^v_{\alpha 1}U^v_{\alpha 2}U^v_{\beta 1}U^v_{\beta 2}\cos\left(2.53\frac{d\,\delta_{21}}{E}\right) +$$
$$2\,U^v_{\alpha 1}U^v_{\alpha 3}U^v_{\beta 1}U^v_{\beta 3}\cos\left(2.53\frac{d\,\delta_{31}}{E}\right) + 2\,U^v_{\alpha 2}U^v_{\alpha 3}U^v_{\beta 2}U^v_{\beta 3}\cos\left(2.53\frac{d\,\delta_{32}}{E}\right), \qquad (15)$$

where d is the distance of travel in meters, δ's are the mass differences in eV^2 and E is the neutrino energy in MeV. Because we have neglected the CP violating phase, the oscillation probability for the anti-neutrinos is the same as that for the neutrinos. Since δ_{21} is very small, the cosine term containing it in eq.(15) can be set equal to 1. The other two cosine terms are dependent on δ_{31} (and $\delta_{32} \simeq \delta_{31}$), the neutrino energy and the distance of travel which is related to the zenith angle. As mentioned earlier, the double ratio R defined in eq.(1) does not have any zenith angle dependence for the sub-GeV data. One can account for this if it is possible to replace the distance dependent terms in eq.(15) by their average values. This replacement is possible only if the average distance travelled contains many oscillation lengths. The above condition sets a lower limit on the mass difference $\delta_{31} > 10^{-3}$ eV^2 [16]. Note that this lower limit is consistent with the approximation $\delta_{31} \gg \delta_{21} \sim 10^{-5}$ eV^2, which was made so that both solar and atmospheric neutrino problems could be solved simultaneously.

$P^0_{\alpha\beta}$ become independent of δ_{31} and the neutrino energy when the distance dependent terms are replaced by their average values. They are simply functions of the mixing angles

ϕ and ψ alone. In this approximation, the expression for the double ratio R can be written as [16]

$$R = \frac{P^0_{\mu\mu} + \frac{1}{r_{MC}}P^0_{e\mu}}{P^0_{ee} + r_{MC}P^0_{\mu e}},\tag{16}$$

where r_{MC} is the Monte Carlo expectation of the ratio of number μ-like events to the number of e-like events. From the sub-GeV data of Kamiokande, we find $r_{MC} = 1.912$ and $R = 0.60^{+0.07}_{-0.06}\pm0.05$ [5,16]. We take the allowed values of ϕ from our analysis of solar neutrino data which restricts ϕ to be in the range $0 \leq \phi \leq 50^0$ [16]. We find the allowed region in the $\phi - \psi$ plane by requiring the theoretical value calculated from eq.(16) to be within 1σ or 1.6σ uncertainty of the experimental value. In our previous analysis we restricted the range of ψ to be $0 \leq \psi \leq 45^0$. However, given the assumptions we made about vacuum mass eigenvalues, the most general possibility is to allow ψ to vary between 0 and 90^0 [20]. The new region allowed by the sub-GeV data, where ϕ was restricted by the solar neutrino data and ψ is allowed to vary between 0 to 90^0, is shown in Figure 1. The region between the solid lines is the parameter space which satisfies the experimental constraints at 1σ level whereas the region between dashed lines satisfies the experimental constraints at 1.6σ level. One important point to be noted in this analysis is that the sub-GeV data place only lower bound on δ_{31}. The allowed region in $\phi - \psi$ plane is quite large.

B. Multi-GeV data

The multi-GeV data of Kamiokande have been presented for five zenith angle bins in Ref. [6]. For each of these bins, the observed numbers of electron-like events and muon-like events and their Monte Carlo expectations (without neutrino oscillations) have been given. From these one can calculate two sets of ratios

$$r^i_{MC} = \left(\frac{N^i_\mu}{N^i_e}\right)_{MC}\tag{17}$$

$$r^i_{obs} = \left(\frac{N^i_\mu}{N^i_e}\right)_{obs},\tag{18}$$

and the set of double ratios

$$R^i_{obs} = r^i_{obs}/r^i_{MC} \tag{19}$$

for each bin $i = 1, 2, ..., 5$. We summarize the multi-GeV data of Kamiokande [6] in Table I.

The μ-like events are subdivided into fully contained (FC) and partially contained (PC) events whereas all the e-like events are fully contained. The efficiency of detection for each type of event is different and is a funtion of the neutrino energy. Thus we have three detection efficiencies $\varepsilon^\mu_{FC}(E)$, $\varepsilon^\mu_{PC}(E)$ and $\varepsilon^e(E)$. We obtained these efficiencies from Kamiokande Collaboration [21].

The expected number of μ-like and e-like events, in the absence of neutrino oscillations, is given by

$$N^i_\mu|_{M.C.} = \int \left[\phi^i_{\nu_\mu}(E)\sigma(E) + \phi^i_{\bar{\nu}_\mu}(E)\bar{\sigma}(E) \right] (\varepsilon^\mu_{FC}(E) + \varepsilon^\mu_{PC}(E)) \, dE \tag{20}$$

$$N^i_e|_{M.C.} = \int \left[\phi^i_{\nu_e}(E)\sigma(E) + \phi^i_{\bar{\nu}_e}(E)\bar{\sigma}(E) \right] \varepsilon^e(E) dE \tag{21}$$

where ϕ's are the fluxes of the atmospheric neutrinos at the location of Kamiokande. These are tabulated in Ref. [1] as functions of the neutrino energy (from $E = 1.6$ GeV to $E = 100$ GeV) and the zenith angle. σ and $\bar{\sigma}$ are the charged current cross sections of neutrinos and anti-neutrinos respectively with nucleons. The cross section is the sum of the quasi-elastic scattering and the deep inelastic scattering (DIS). The values for quasi-elastic scattering are taken from Gaisser and O'Connel [22] and those for the DIS are taken from Gargamelle data [23]. In calculating the DIS cross section, we took the lepton energy distribution to be given by the scaling formula (which is different for neutrinos and anti-neutrinos) and integrated $d\sigma/dE_{lep}$ from the minimum lepton energy $E_{min} = 1.33$ GeV to the maximum lepton energy $E_{max} = E_\nu - m_\pi$. The maximum lepton energy is chosen by defining DIS to contain at least one pion in addition to the charged lepton and the baryon. The differences in the fiducial volumes and exposure times for fully contained and partially contained events have been incorporated into the detection efficiency $\varepsilon^\mu_{PC}(E)$. From equations (20) and (21) we calculate our estimation of the Monte Carlo expectation of r^i_{MC}, the ratio of the μ-like

10

events to the e-like events. The numbers we obtain are within 10% of the values quoted by Kamiokande collaboration in Ref. [6]. The differences could be due to the different set fluxes used [24] and due to the simple approximation we made for the cross sections.

In the presence of oscillations, the number of μ-like and e-like events are given by

$$N_\mu^i|_{osc} = \int \left[\phi_{\nu_\mu}^i P_{\mu\mu}\sigma + \phi_{\bar{\nu}_\mu}^i P_{\bar{\mu}\bar{\mu}}\bar{\sigma} + \phi_{\nu_e}^i P_{e\mu}\sigma + \phi_{\bar{\nu}_e}^i P_{\bar{e}\bar{\mu}}\bar{\sigma} \right] (\varepsilon_{FC}^\mu + \varepsilon_{PC}^\mu)\, dE \tag{22}$$

$$N_e^i|_{osc} = \int \left[\phi_{\nu_e}^i P_{ee}\sigma + \phi_{\bar{\nu}_e}^i P_{\bar{e}\bar{e}}\bar{\sigma} + \phi_{\nu_\mu}^i P_{\mu e}\sigma + \phi_{\bar{\nu}_\mu}^i P_{\bar{\mu}\bar{e}}\bar{\sigma} \right] \varepsilon^e\, dE \tag{23}$$

where $P_{\alpha\beta}$s are the probabilities for neutrino of flavor α to oscillate into flavor β, derived in the last section. These oscillation probabilities are functions of the distance of travel d, the mixing angles ϕ and ψ, the mass difference δ_{31} and the matter term A. These are calculated using the formulae in eqs. (8), (9), (10) and (14). The probability of oscillation for anti-neutrinos $P_{\bar{\alpha}\bar{\beta}}$, in general, is different from $P_{\alpha\beta}$ because of the different A dependence.

From equations (22) and (23) we can calculate the ratio of μ-like events to e-like events in the presence of oscillations to be

$$r_{osc}^i = \left(\frac{N_\mu^i}{N_e^i} \right)_{osc} \tag{24}$$

and the double ratio

$$R_{osc}^i = \frac{r_{osc}^i}{r_{MC}^i}. \tag{25}$$

If the atmospheric neutrino deficit is due to neutrino oscillations, then the double ratios R_{osc}^i given in eq. (25) should be within the range of the corresponding observed double ratios R_{obs}^i, which are given in Table I. We searched for the values of the neutrino parameters ϕ, ψ and δ_{31} for which the predicted values of R_{osc}^i satisfy the experimental constraints on the double ratios for all the five bins. The ranges of variation in the three parameters are

1. $0 \leq \phi \leq 50^0$. This is the range of ϕ allowed by the solar neutrino problem. For this range of ϕ, there exist values of δ_{21} and ω such that all the three solar neutrino experiments can be explained [16,25].

11

2. $0 \leq \psi \leq 90^0$. ψ is varied over its fully allowed range.

3. $10^{-3}\ eV^2 \leq \delta_{31} \leq 10^{-1}\ eV^2$. The lower limit is given by the sub-GeV data and the upper limit is the largest value allowed by the two flavor analysis of the multi-GeV data by Kamiokande [6].

The results are plotted in Figures 2, 3 and 4. Figure 2 gives the projection of the allowed region on the $\phi - \psi$ plane, Figure 3 gives the projection on the $\phi - \delta_{31}$ plane and Figure 4 gives the projection on the $\psi - \delta_{31}$ plane. The solid lines enclose the regions of parameter space whose predictions lie within the experimental range given by 1σ uncertainties. The broken lines enclose regions whose predictions fall within range given by 1.6σ uncertainties.

As seen from Table I, the uncertainties in bin 5, which has $\langle \cos \theta \rangle = 0.8$, are quite large compared to the uncertainties in the other four bins. Morevoer, r^5_{obs} is greater than r^5_{MC} through most of its range. Hence the double ratio $R^5_{obs} > 1$ for most of its range. The Monte Carlo expectation of the electron neutrino flux is less than that of the muon neutrino flux and the oscillation probabilities $P_{\alpha\beta}$ are all less than 1. Using these facts, one can show from eqs. (17) and (24) that, in general, $r^i_{osc} \leq r^i_{MC}$ or $R^i_{osc} \leq 1$. Therefore, the region of overlap between R^5_{obs} and R^5_{osc} is very small. It is $0.9 - 1.0$ for 1σ uncertainties. It is possible that this small overlap is imposing a very strong constraint, leading to a situation where the bin with the largest uncertainty is essentially controlling the allowed values of the parameters. Because of this unsatisfactory situation, we redid the analysis ignoring the constraint from bin 5. We searched for regions of parameter space for which the values of R^i_{osc} are within the ranges of corresponding R^i_{obs} for only the first four bins.

The results of the 4 bin analysis are plotted in Figures 5, 6 and 7. Figure 5 gives the projection of the allowed region on the $\phi - \psi$ plane, Figure 6 gives the projection on the $\phi - \delta_{31}$ plane and Figure 7 gives the projection on the $\psi - \delta_{31}$ plane. As before, the solid lines enclose the regions satisfying 1σ vetoes and the broken lines enclose regions allowed by 1.6σ vetoes. Comparing the corresponding figures we find that the allowed values of parameters for the 4 bin fit are the almost identical to those from the 5 bin fit at 1.6σ level. The allowed

regions at 1σ level are somewhat larger compared to the 5 bin fit. This is not surprising because the bin 5 imposes a very strong constraint at 1σ level. If this constraint is relaxed, then a somewhat larger region is allowed. The 4 bin fit shows that the 5th bin, which has the largest uncertainty, does not exercise undue influence on the selection of the parameter space.

IV. DISCUSSION AND CONCLUSIONS

The parameter space shown in Figures 1 to 4 , together with the allowed values for ω and δ_{21} from our earlier work [16], provides a complete solution to the solar and the atmospheric neutrino problems in the framework of three flavor neutrino oscillations. The salient features of the results of the multi-GeV analysis are:

- Most of the parameter space allowed by the multi-GeV data is a subset of the space allowed by the sub-GeV data.

- The range of δ_{31} allowed by 1σ vetoes is extremely narrow. It is very close to the best fit value given by the two flavor analysis of Kamiokande.

- The value of ψ is always large ($\psi \geq 40^0$) and $\psi = 90^0$ is allowed.

- In the region allowed by 1σ vetoes ϕ is always non-zero. $\phi = 0$ is allowed only at 1.6σ vetoes.

From the parametrization of U^v, effective two level mixings can be obtained for the following choices of the angles:

- $\nu_e \leftrightarrow \nu_\mu$ for $\psi = 90^0$,

- $\nu_e \leftrightarrow \nu_\tau$ for $\psi = 0$ and

- $\nu_\mu \leftrightarrow \nu_\tau$ for $\phi = 0$.

Any solution to the atmospheric neutrino problem should suppress the muon neutrinos, enhance the electron neutrinos or do both. The $\nu_e \leftrightarrow \nu_\tau$ channel, which suppresses electron neutrinos but leaves muon neutrinos untouched, cannot account for the atmospheric neutrino problem. Hence any solution of atmospheric neutrino problem should be away from the effective two flavor $\nu_e \leftrightarrow \nu_\tau$ oscillations. The large value of the angle ψ is just a reflection of this fact. The allowed region includes the value $\psi = 90^0$. Then the atmospheric neutrino problem is explained purely in terms of the two flavor oscillations between $\nu_e \leftrightarrow \nu_\mu$, with the relevant mass difference being δ_{31}. In this case, the solar neutrino problem is solved by $\nu_e \to \nu_\tau$ oscillation which is determined by the mass difference δ_{21} (and the mixing angles ω and ϕ).

How important are the matter effects in the analysis of the multi-GeV data? It can be seen from figures 2(d)-2(f) of Ref. [6] that most of the expected multi-GeV events are caused by neutrinos with energies less than 10 GeV (over 80% for muon-like events and over 90% for electron-like events). The matter term, for a neutrino of energy 5 GeV, is about $2 \times 10^{-3} eV^2$. Since the initial range we considered for δ_{31} varied from $10^{-3}\ eV^2$ to 0.1 eV^2, apriori one must include the matter effects in the expressions for the oscillation probabilities. However, the value of δ_{31} in the allowed region, especially for the 1σ vetoes, where it is about 0.03 eV^2, is much larger than the matter term. Therefore, it is likely that the matter effects may not play an important role in determining the allowed parameter regions in the analysis of the multi-GeV data. To check this we reran our program with the matter term set equal to zero. With this change, the double ratios R_{osc}^i, defined in equation (24), changes by about 10% in the first bin and by about 5% in the second bin. There is no discernible change in the other three bins. Since the errors in R_{obs}^i are about 30%, these small changes in R_{osc}^i do not lead to any apprecialble change in the allowed regions of the parameter space. However, the effect of matter terms may become discerible when more accurate data from Super Kamiokande become available.

Since the earth matter effects seem to play no role in the determination of the parameter space, can one interpret the observed zenith angle dependence purely in terms of vacuum

14

oscillations? For an energy of 5 GeV, the mass square difference 10^{-2} eV^2 corresponds to an oscillation length of about 1200 Km. Thus bins 1 and 2 contain many oscillation lengths and the second and the third cosine terms in the vacuum oscillation probability, given in equation (15), average out to zero. For bins 4 and 5 the cosine terms are almost 1. In bin 3, these terms take some intermediate value. Therefore we have large suppression in the first two bins, almost no suppression in the last two bins and moderate suppression in the middle bin.

Eventhough matter terms play no important role in the multi-GeV analysis, $\nu_e \leftrightarrow \nu_\mu$ oscillations provide a better fit to data compared to $\nu_\mu \leftrightarrow \nu_\tau$ oscillations. In $\nu_\mu \leftrightarrow \nu_\tau$ oscillations, the ν_μ flux is suppressed whereas the ν_e flux is untouched. Thus the double ratios R_{osc}^i do become less than 1 but the large suppression observed in bins 1 and 2 is difficult to achieve via this channel. For $\nu_e \leftrightarrow \nu_\mu$ oscillations, the ν_μ flux is reduced and ν_e flux is increased. This occurs even when $P_{\mu e} = P_{e\mu}$, which is the case for vacuum oscillations, because the flux of ν_μ is roughly twice the flux of ν_e before oscillations. Hence the double ratios R_{osc}^i are smaller for the case of $\nu_e \leftrightarrow \nu_\mu$ oscillations compared to the case of $\nu_\mu \leftrightarrow \nu_\tau$ oscillations and they fit the data better.

We now make a brief comment on the LSND results on the search for $\bar{\nu}_\mu \rightarrow \bar{\nu}_e$ oscillations [18] in the context of our analysis of atmospheric neutrinos. The LSND collaboration gives an oscillation probability $P_{\bar{\mu}\bar{e}} = (3.1^{+1.1}_{-1.0} \pm 0.5) \times 10^{-3}$ for muon anti-neutrinos in the energy range $20 - 60$ MeV. In the framework described in section II, the oscillation probability relevant for the LSND experiment is the vacuum oscillation probability

$$P_{\bar{\mu}\bar{e}}^0 = P_{\mu e}^0 = \sin^2 2\phi \sin^2 \psi \sin^2 \left(1.27 \frac{d\,\delta_{31}}{E} \right). \tag{26}$$

Note that both ϕ and ψ have to be non-zero for $P_{\mu e}$ to be non-zero. In the region allowed by the 1σ vetoes of the multi-GeV atmospheric neutrino data we have

$$\text{Minimum } \left(\sin^2 2\phi \sin^2 \psi \right) \simeq 0.04 \text{ for } \phi \simeq 8^0, \psi \simeq 40^0$$

$$\text{Maximum } \left(\sin^2 2\phi \sin^2 \psi \right) \simeq 1 \text{ for } \phi \simeq 40^0, \psi \simeq 90^0.$$

15

Substituting these values and the oscillation probability obtained by LSND in eq. (26), we obtain

$$0.001 \le \sin^2\left(1.27\frac{d\,\delta_{31}}{E}\right) \le 0.1. \tag{27}$$

For the LSND experiment the distance $d = 30$ meters. Taking the average energy to be $\langle E \rangle = 40$ MeV, we obtain the range of δ_{31} to be

$$0.03 \; eV^2 \le \delta_{31} \le 0.3 \; eV^2. \tag{28}$$

From the analysis of multi-GeV atmospheric neutrino data we have the upper limit on $\delta_{31} \le 0.06 \; eV^2$ (Figures 3 and 4). Hence there is a small region of overlap between the range of neutrino parameters required by the atmospheric neutrino data and the LSND data. This suggests that the standard three flavor analysis can accommodate all the data so far [26] and perhaps a fourth sterile neutrino is not needed.

In conclusion, we have analyzed the atmospheric neutrino data of Kamiokande in the context of three flavor neutrino oscillations. We took into account both the zenith angle dependence of the multi-GeV data and the matter effects due to the propagation of the neutrinos through the earth. We obtained the regions in neutrino parameters which solve both the solar and the atmospheric neutrino problems. We found that the matter effects have negligible influence on atmopsheric neutrinos even in the multi-GeV range. The allowed regions of the parameter space with or without matter effects are almost identical.

As we finished this work, we came across a preprint by Fogli *et al* [27]. They have analyzed the sub-GeV data from various experiments and the zenith angle dependent multi-GeV data from Kamiokande. Although a detailed comparison is difficult, qualitatively our results agree with theirs.

REFERENCES

[1] M. Honda *et al*, Phys. Rev. **D52**, 4985 (1995).

[2] V. Agrawal *et al*, Phys. Rev. **D53**, 1314 (1996).

[3] IMB Collaboration: D. Casper *et al.*, Phys. Rev. Lett. **66**, 2561(1991); R. Becker-Szendy *et al.*, Phys. Rev. **D46**, 3720(1992).

[4] IMB Collaboration observed a deficit of muon-like events in their data compared to the Monte-Carlo prediction as early as 1986 and have speculated whether this deficit is due to non-Standard Physcis. T. J. Haines *et al*, Phys. Rev. Lett. **57**, 1986 (1986).

[5] Kamiokande Collaboration: K. S. Hirata *et al*, Phys. Lett. **B280**, 146 (1992).

[6] Kamiokande Collaboration: Y. Fukuda *et al*, Phys. Lett. **B335**, 237 (1994).

[7] V. Barger *et al*, Phys. Rev. **D22**, 2718 (1980).

[8] G. V. Dass and K. V. L. Sarma, Phys. Rev. **D30**, 80 (1984).

[9] J. Pantaleone, Phys. Rev. **D49**, R2152 (1994).

[10] S. Goswami, K. Kar and A. Raychaudhury, CUPP-95/3 May 1995, hep-ph/9505395; S. Goswami, CUPP-95/4 July 1995, hep-ph/9507212.

[11] S. M. Bilenky, C. Giunti and C. W. Kim, hep-ph 9505301.

[12] C. Giunti, C. W. Kim and J. D. Kim, Phys. Lett. **352B**, 357 (1995).

[13] D. Harley, T. K. Kuo and J. Pantaleone, Phys. Rev. **D47**, 4059 (1993).

[14] G. Fogli, E. Lisi and D. Montanino, Phys. Rev. **D49**, 3626 (1994); Astropart. Phys. **4**, 177 (1995).

[15] A. S. Joshipura and P. I. Krastev, Phys. Rev. **D 50**, 3484 (1994).

[16] M. Narayan *et al*, Phys. Rev. **D53**, 2809 (1996).

[17] O. Yasuda, TMUP-HEL-9603 February 1996, hep-ph/9602342

[18] LSND Collaboration: C. Athanassopoulos *et al*, Los Alamos Preprint LA-UR-96-1582, nucl-ex/9605003.

[19] L. Wolfenstein, Phys. Rev. **D17**, 2369 (1978); **D20**, 2634 (1979).

[20] We thank J. Pantaleone for pointing this out to us.

[21] We thank Prof. T. Kajita of the Kamiokande Collaboration for providing us with the efficiencies for the detection of various types of events.

[22] T. K. Gaisser and J. S. O'Connell, Phys. Rev **D34**, 822 (1986).

[23] P. Musset and J. P. Vialle, Phys. Rep. **39C**, 1 (1978).

[24] Kamiokande Collaboration, in their analysis in Ref. [6], used the fluxes from G. Barr, T. K. Gaisser and T. Stanev, Phys. Rev. **D39**, 3532 (1989) for $e_\nu < 3\ GeV$ and those from L. V. Volkova, Sov. J. Nucl. Phys. **31**, 784 (1980) for $E_\nu > 10\ GeV$. For energies between 3 and 10 GeV they have smoothly interpolated between the two fluxes.

[25] G. L. Fogli, E. Lisi and D. Montanino, Phys. Rev. **D54**, 2048 (1996).

[26] C. Y. Cardall and G. M. Fuller, Phys. Rev. **D53**, 4421 (1996).

[27] G. L. Fogli, E. Lisi, D. Montanino and G. Scioscia, Preprint Number IASSNS-AST-96/41, hep-ph/9607251.

TABLES

Bin No.	$\langle cos\theta \rangle$	$\langle distance \rangle$ in Km	r^i_{MC}	r^i_{obs}	R^i_{obs}
1	-0.8	10,210	3.0	$0.87^{+0.36}_{-0.21}$	$0.29^{+0.12}_{-0.07}$
2	-0.4	5,137	2.3	$1.06^{+0.39}_{-0.30}$	$0.46^{+0.17}_{-0.13}$
3	0.0	832	2.1	$1.07^{+0.32}_{-0.23}$	$0.51^{+0.15}_{-0.11}$
4	0.4	34	2.3	$1.45^{+0.51}_{-0.34}$	$0.63^{+0.22}_{-0.16}$
5	0.8	6	3.0	$3.9^{+1.8}_{-1.2}$	$1.3^{+0.6}_{-0.4}$

TABLE I. Zenith angle dependent data from Kamiokande [6]

FIGURES

FIG. 1. Allowed region in $\phi - \psi$ plane by the sub-GeV data (with $\delta_{31} \geq 10^{-3}\ eV^2$) at 1σ (enclosed by solid lines) and at 1.6σ (enclosed by broken lines)

FIG. 2. Allowed region in $\phi - \psi$ plane by 5 bin analysis of multi-GeV data (with $10^{-3}\ eV^2 \leq \delta_{31} \leq 10^{-1}\ eV^2$) at 1σ (enclosed by solid lines) and at 1.6σ (enclosed by broken lines)

FIG. 3. Allowed region in $\phi - \delta_{31}$ plane by 5 bin analysis of multi-GeV data (with $0 \leq \psi \leq 90^0$) at 1σ (enclosed by solid lines) and at 1.6σ (enclosed by broken lines)

FIG. 4. Allowed region in $\psi - \delta_{31}$ plane by 5 bin analysis of multi-GeV data (with $0 \leq \phi \leq 50^0$) at 1σ (enclosed by solid lines) and at 1.6σ (enclosed by broken lines)
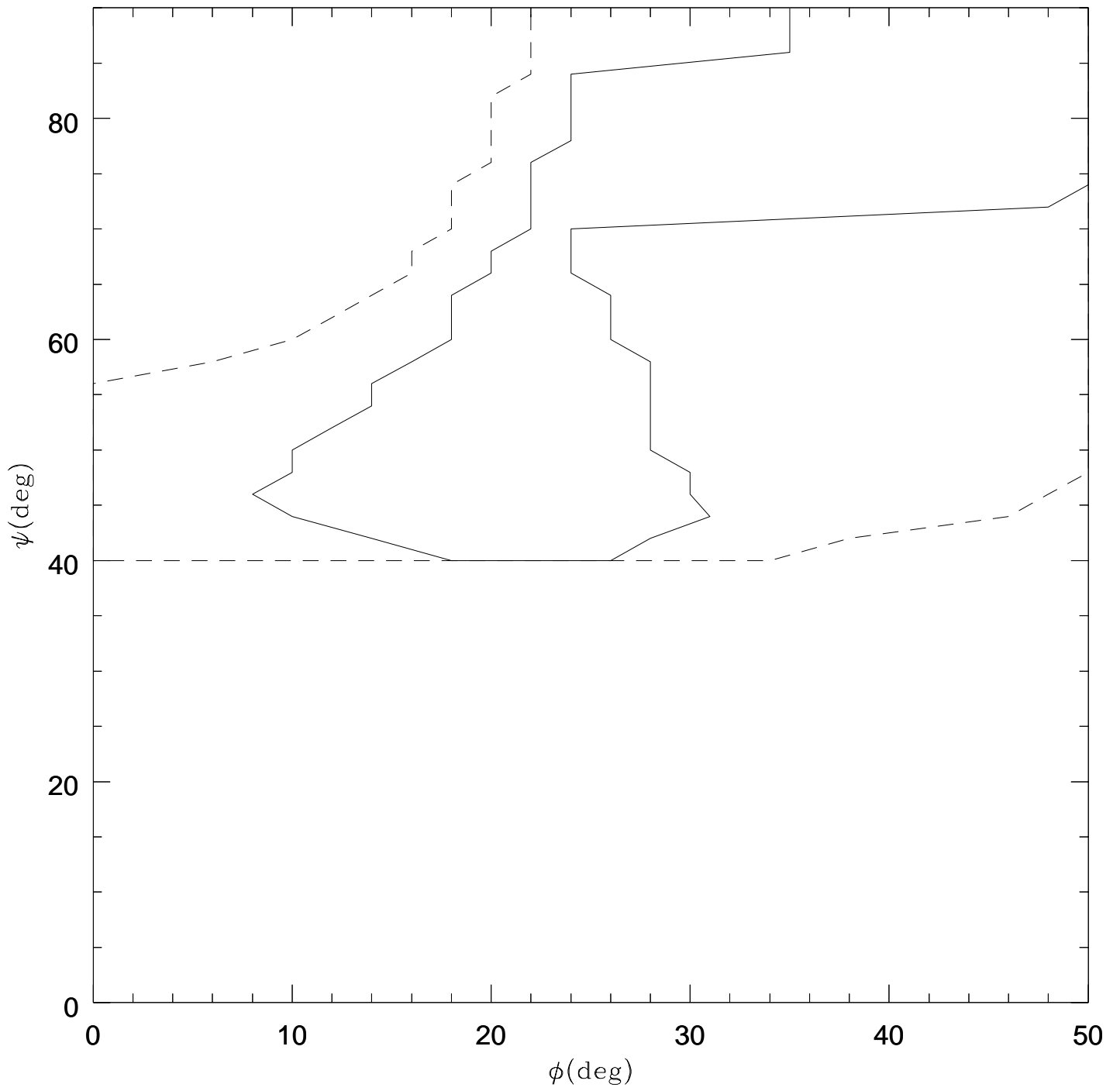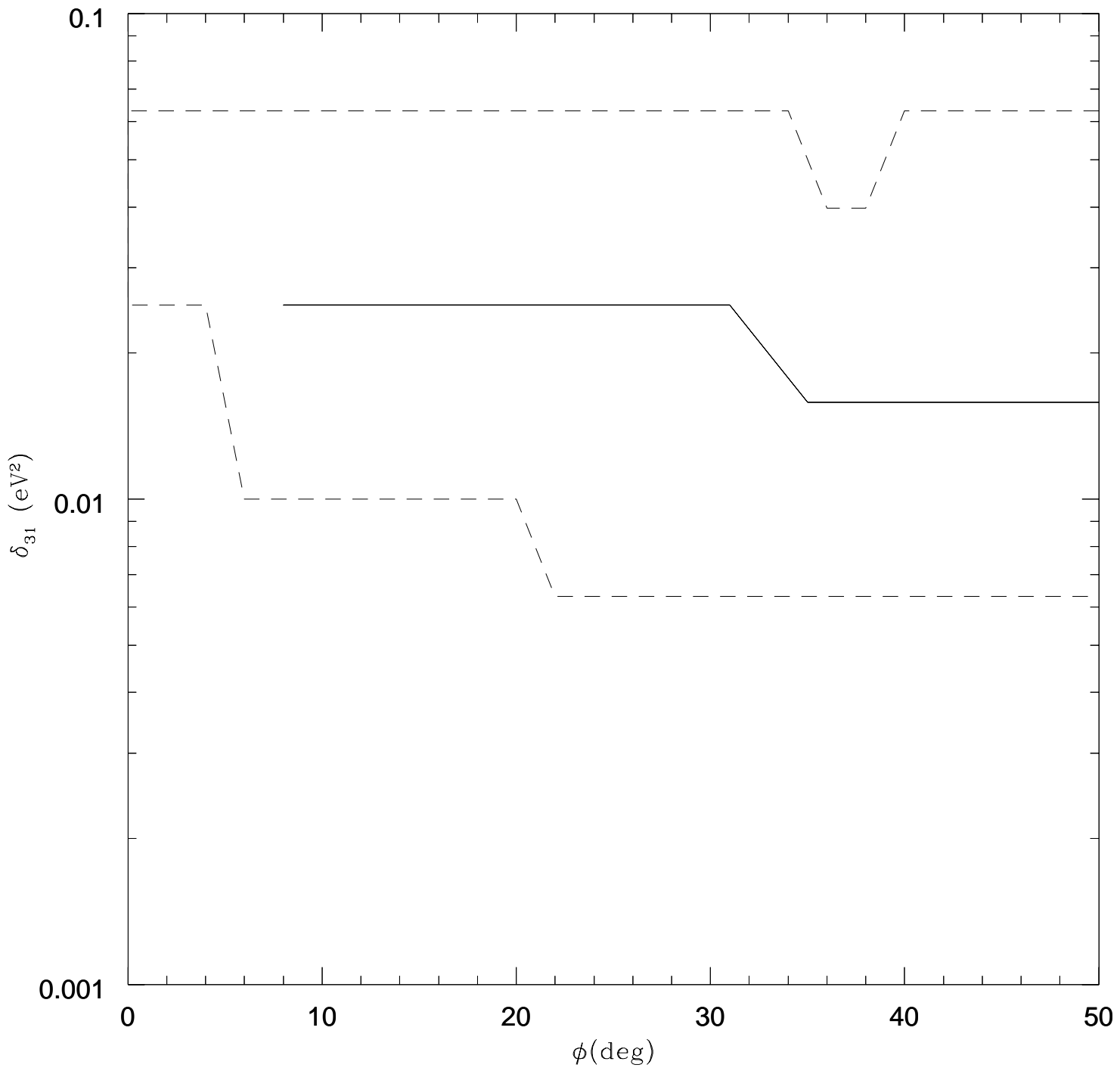
FIG. 5. Allowed region in $\phi - \psi$ plane by 4 bin analysis of multi-GeV data (with $10^{-3}\ eV^2 \leq \delta_{31} \leq 10\ eV^2$) at 1σ (enclosed by solid lines) and at 1.6σ (enclosed by broken lines)

FIG. 6. Allowed region in $\phi - \delta_{31}$ plane by 4 bin analysis of multi-GeV data (with $0 \leq \psi \leq 90^0$) at 1σ (enclosed by solid lines) and at 1.6σ (enclosed by broken lines)

FIG. 7. Allowed region in $\psi - \delta_{31}$ plane by 4 bin analysis of multi-GeV data (with $0 \leq \phi \leq 50^0$) at 1σ (enclosed by solid lines) and at 1.6σ (enclosed by broken lines)
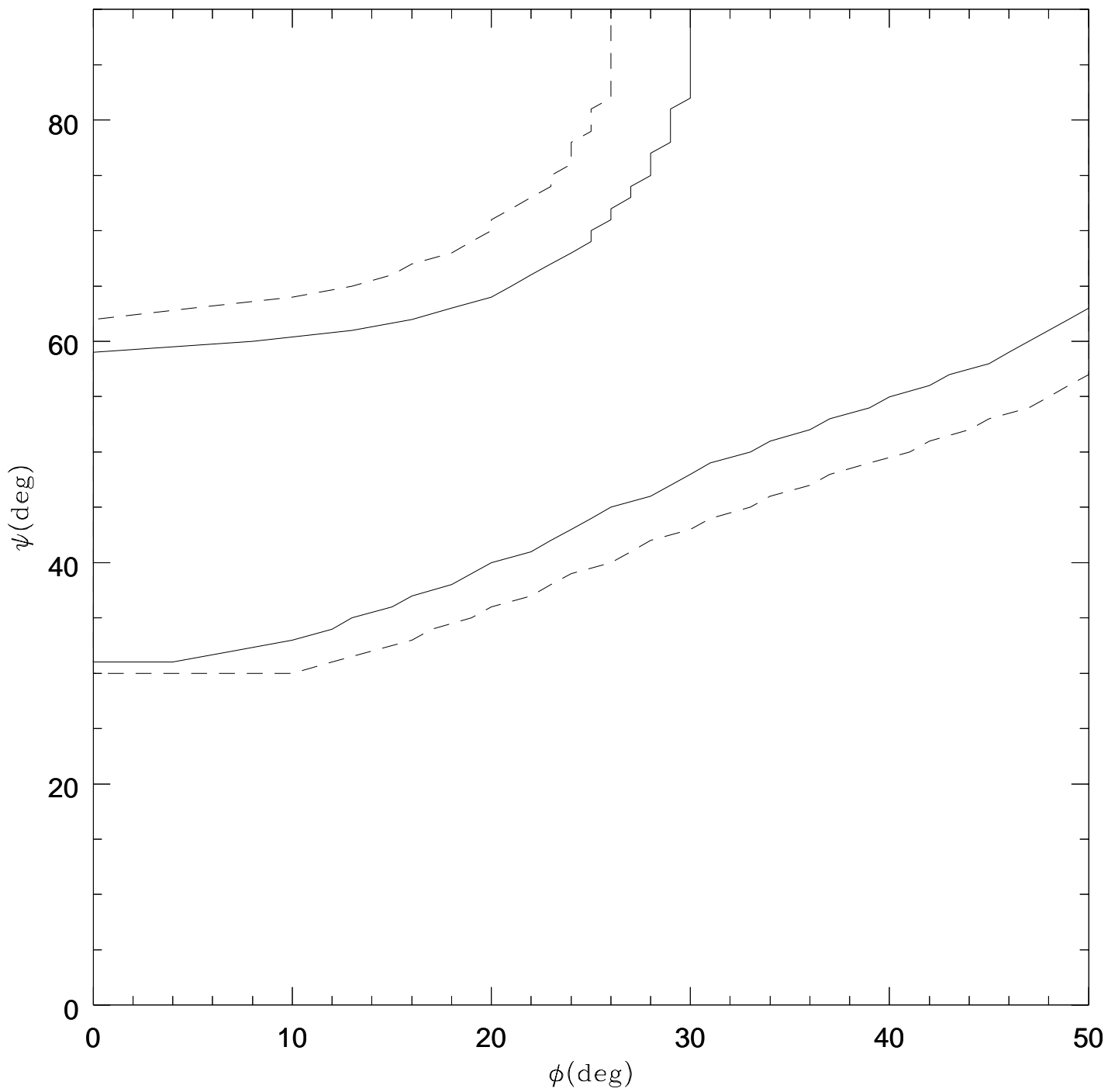
Fig1

Fig2

Fig3

Fig4

Fig5

Fig6

Fig7